J. Fluid Mech. (2008), *vol.* 616, *pp.* 235–262.
doi:10.1017/S0022112008003790 Printed in the United Kingdom

The thinning of lamellae in surfactant-free foams with non-Newtonian liquid phase

L. N. BRUSH[1] AND S. M. ROPER[2]

[1]Department of Materials Science and Engineering, University of Washington, Seattle, WA 98195, USA
brush@u.washington.edu

[2]Department of Mathematics, University of Glasgow, Glasgow, UK
sroper@maths.gla.ac.uk

(Received 9 August 2007 and in revised form 31 July 2008)

Thinning rates of liquid lamellae in surfactant-free non-Newtonian gas–liquid foams, appropriate for ceramic or polymer melts and also in metals near the melting point, are derived in two dimensions by matched asymptotic analysis valid at small capillary number. The liquid viscosity is modelled (i) as a power-law function of the shear rate and (ii) by the Ellis law. Equations governing gas–liquid interface dynamics and variations in liquid viscosity are derived within the lamellar, transition and plateau border regions of a corner of the liquid surrounding a gas bubble. The results show that the viscosity varies primarily in the very short transition region lying between the lamellar and the Plateau border regions where the shear rates can become very large. In contrast to a foam with Newtonian liquid, the matching condition which determines the rate of lamellar thinning is non-local. In all cases considered, calculated lamellar thinning rates exhibit an initial transient thinning regime, followed by a t^{-2} power-law thinning regime, similar to the behaviour seen in foams with Newtonian liquid phase. In semi-arid foam, in which the liquid fraction is $O(1)$ in the small capillary number, results explicitly show that for both the power-law and Ellis-law model of viscosity, the thinning of lamella in non-Newtonian and Newtonian foams is governed by the same equation, from which scaling laws can be deduced. This result is consistent with recently published experimental results on forced foam drainage. However, in an arid foam, which has much smaller volume fraction of liquid resulting in an increase in the Plateau border radius of curvature as lamellar thinning progresses, the scaling law depends on the material and the thinning rate is not independent of the liquid viscosity model parameters. Calculations of thinning rates, viscosities, pressures, interface shapes and shear rates in the transition region are presented using data for real liquids from the literature. Although for shear-thinning fluids the power-law viscosity becomes infinite at the boundaries of the internal transition region where the shear rate is zero, the interface shape, the pressure and the internal shear rates calculated by both rheological models are indistinguishable.

1. Introduction

A gas–liquid foam is a composite of gas bubbles in a liquid matrix, in which the volume fraction of the gas is large enough that the bubbles are not spherical. As a result, adjacent gas bubbles in the foam are separated by nearly flat thin liquid lamellar films. The Plateau borders are the intersections of many lamellar films, and are bounded by curved gas–liquid interfaces (see figure 1). The change in

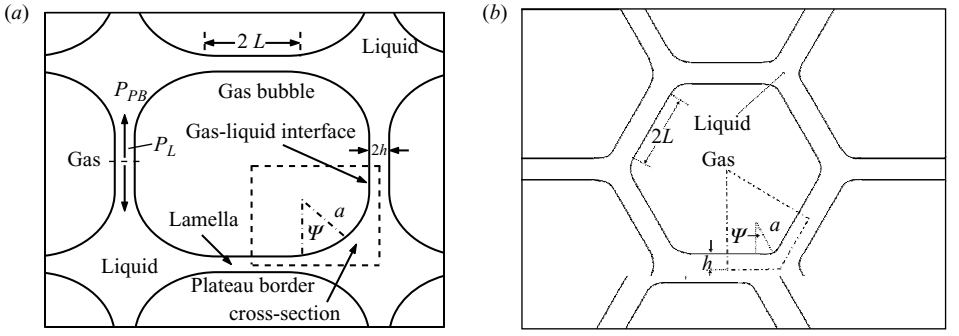

FIGURE 1. Schematic representation of the cross-section of a foam for (*a*) a square array and (*b*) an hexagonal array of bubbles, showing a set of adjacent gas bubbles and the lamellar, transition and Plateau border regions. The dot-dash lined sections within each diagram are the periodic domains within which asymptotic analyses are carried out for each geometry. The symmetry of the array of bubbles fixes the angle Ψ: $\Psi = \pi/4$ in (*a*) and $\pi/6$ in (*b*) (Brush & Davis 2005).

curvature of a bubble gas–liquid interface while moving from a flat lamellar region into a curved Plateau border region leads to fluid flow from the lamella into the Plateau borders. Depending on the foam configuration, fluid may then travel along the Plateau borders and eventually out of the foam into a liquid reservoir. The fluid flowing from the lamella into the Plateau borders results in thinning of the lamella which, when accompanied by instability of the film, can lead to lamellar rupture and the coalescence of neighbouring bubbles. The focus of this paper is the calculation of lamellar thinning rates in foams having non-Newtonian liquid phase.

A wide variety of liquids may be foamed. Thinning rates and rupture times depend strongly on the types of liquids involved. In pure metallic foams and in aqueous solutions, the rupture time of liquid lamella can be milliseconds. In aqueous-like liquids, surfactant can be added to lower the gas–liquid surface tension and decrease the thinning rates by orders of magnitude (Breward 1999; Breward & Howell 2002). Surfactants are not available to affect the surface tension of metallic foams. Therefore, particles, compounds or other substances are often added to metallic foam to increase the apparent liquid viscosity and to slow down the rupture process (Banhart 2001; Yang & Nakae 2003). Ceramic foams are produced from polymer melts by the condensation and the reaction products formed during cross-linking (Scheffler *et al.* 2002). The dynamics of the polymer foams are strongly dependent on the temperature. In a related problem, the draining of liquid layers surrounding gas bubbles in glass melts with high viscosity have been studied by Howell (1999). Recently, Safouane *et al.* (2006) have reported forced drainage experiments in shear-thinning foam solutions in which the solution viscosity is carefully controlled. The results showed that the dynamics of liquid drainage in a foam with a shear-thinning liquid solution are identical to the drainage of foam having a Newtonian liquid if an effective viscosity based on an estimated shear rate within the foam is used. As we shall see, our results provide quantitative estimates for this class of foams which corresponds to one of two asymptotic limits.

Foams are three-dimensional networks of nodes, Plateau borders and lamellae, so that flow within foam and the dynamics of foams is three-dimensional. However, lamella span the Plateau borders and the nodes and, being free films, are nearly uniform layers of liquid. Moreover, Plateau borders are the intersections of lamellae

that generally appear to be uniform in the axial direction. Therefore, the flow of fluid from the lamella into the Plateau borders and the thinning of the lamella should be well approximated by a two-dimensional section parallel to the thin direction through the lamella and perpendicular to the axial Plateau border orientation. Depending on the foam configuration, fluid may then travel along the Plateau borders and eventually out of the foam into bulk liquid. Although flow does occur along the axial direction of the Plateau border, because of gravitational and other forces, it is not anticipated that this flow will play a role in altering the thinning rates of the lamella.

A complete description of the evolution of a foam would couple the drainage of lamellae to Plateau borders (Breward & Howell 2002; Brush & Davis 2005) to the drainage of fluid along the network of Plateau borders (Wang & Narsimhan 2006) and finally to the interaction with any surrounding bulk fluid/solid. The work in this paper could be coupled with that of Wang & Narsimhan to construct a model for foam drainage.

Previously, thinning rates of lamella have been calculated in foams with Newtonian liquid phases. Breward & Howell (2002) calculated foam thinning rates in pure and surfactant-laden foams using matched asymptotic analysis. They examined the effect of surfactant, among other effects, on the thinning rates. In their work, the radius of curvature of the Plateau border is assumed fixed, i.e. the volume of fluid leaving the lamella is not enough to cause displacement of the Plateau border.

Brush & Davis (2005) have extended this work for surfactant-free foams, to the case in which the Plateau border radius of curvature can also be time dependent. This case corresponds to a leading-order asymptotic limit of much smaller liquid fraction, in which the area of fluid in the Plateau border cross-section is the same order of magnitude as that in the lamella. Therefore, as thinning occurs, the Plateau border radius must increase in order to accommodate incoming liquid flowing from the lamella. Brush & Davis (2005) have defined the foam with a fixed Plateau border radius as a semi-arid foam and the foam with a dynamic Plateau border as an arid foam.

In this work, the effect of variations in the viscosity of the liquid phase on the dynamics of lamellar thinning in a foam is considered. In particular, we consider the case of a non-Newtonian fluid with liquid viscosity modelled (i) as a power-law function of the local shear rate and (ii) by the Ellis model. (Models that include variable viscosity in the equations of motion and continuity with no other modifications, are also referred to as generalized Newtonian fluid models.) These models have been chosen because Rosenblatt & Davis (1984) have shown that if a full rheological model is used, such as a generalized Maxwell constitutive equation which includes the shear dependence of viscosity, normal stress differences in the liquid and relaxation times in the liquid, then, to leading order in the capillary number, the only effect that emerges is the shear rate dependence of the viscosity. This latter effect is appropriately included in the models presented here. (In this paper, foams are labelled as Newtonian or non-Newtonian. It does not mean that the foams have this rheological behaviour, but that the liquid phase of the foam behaves in this manner.)

It is also noted that there exists a model of fluid behaviour with a second Newtonian Plateau for higher shear rates, the Carreau model (Bird *et al.* 1977). In this model the shear thinning or thickening behaviour of the liquid is limited to a range between lower and upper critical values of the shear rate, with Newtonian behaviour observed otherwise. In a foam, the second Newtonian Plateau would occur in an internal layer within the internal transition region layer (which is a very short region itself). Although it would be possible to include a Carreau model of the viscosity, it is

not clear what new insight the model would provide considering the limited region in which there would be high shear rate Newtonian behaviour and considering the difficulty in its implementation.

Therefore, with this analysis the categories of foams considered include Newtonian, non-Newtonian power-law and non-Newtonian Ellis-law types, for the two distinguished asymptotic limits designated as arid and semi-arid foams. The addition of surfactants is not considered in this work.

2. The model

2.1. *Governing equations*

In two dimensions, the equations governing the horizontal and vertical components of the liquid velocities $u(x, z, t)$, $w(x, z, t)$ and the pressure $p(x, z, t)$ are

$$\rho\,(u_t + uu_x + wu_z) = -(p+\phi)_x - \tau_x^{xx} - \tau_z^{xz}, \tag{2.1}$$

$$\rho\,(w_t + uw_x + ww_z) = -(p+\phi)_z - \tau_x^{xz} - \tau_z^{zz}, \tag{2.2}$$

and for incompressible fluid flow

$$u_x + w_z = 0. \tag{2.3}$$

$-\nabla\phi$ is a body force, for example long-range molecular forces, and ρ is the density of the fluid. The superscripted variables in the bulk equations denote components of the shear stress tensor, which for an incompressible fluid is written as

$$\begin{aligned}\overline{\boldsymbol{\tau}} = \begin{pmatrix} \tau^{xx} & \tau^{xz} \\ \tau^{xz} & \tau^{zz} \end{pmatrix} &= -2\eta\{\dot\gamma\} \begin{pmatrix} u_x & \frac{1}{2}\,[u_z + w_x] \\ \frac{1}{2}\,[w_x + u_z] & w_z \end{pmatrix} \\ &= -2\eta\{\dot\gamma\}\overline{\boldsymbol{E}} \quad (= -\eta(\nabla\boldsymbol{v} + \nabla\boldsymbol{v}^T)),\end{aligned} \tag{2.4}$$

where $\eta\{\dot\gamma\}$ is the fluid viscosity which is assumed to depend on the shear rate $\dot\gamma$. The shear rate is given by

$$\dot\gamma^2 = 2\overline{\boldsymbol{E}} : \overline{\boldsymbol{E}} = 2\mathrm{Tr}\,\{\overline{\boldsymbol{E}}^2\} = 2\left(u_x^2 + w_z^2\right) + (u_z + w_x)^2\,, \tag{2.5}$$

where $\mathrm{Tr}\{\cdot\}$ denotes the trace. The power-law model of the viscosity is given by

$$\eta\{\dot\gamma\} = k(\dot\gamma^2)^{(n-1)/2}, \tag{2.6}$$

and the Ellis model by

$$\frac{1}{\eta} = \frac{1}{\eta_0}\left(1 + \left|\frac{\sqrt{1/2\,(\overline{\boldsymbol{\tau}} : \overline{\boldsymbol{\tau}})}}{\tau_{1/2}}\right|^{\alpha-1}\right). \tag{2.7}$$

In the Ellis model, η_0 is the viscosity at zero shear rate, $\overline{\boldsymbol{\tau}}$ is the shear-stress tensor and $\tau_{1/2}$ is the shear stress required to reduce the liquid viscosity to a value of $\eta_0/2$.

Values of the parameters used in the power-law and the Ellis model are given in the literature for a variety of fluids (Bird *et al.* 1977; Myers 2005). The Ellis model has a constant viscosity for shear rates that are sufficiently low, and so behaves as a Newtonian fluid in the low-shear-rate regime. As the shear rate increases beyond a critical value, there is a transition to power-law behaviour which persists for all greater shear rates.

At the gas–liquid interface $z = h(t, x)$, the kinematic condition is

$$w = h_t + uh_x. \tag{2.8}$$

The normal stress balance leads to

$$-p + p_{ext} - \left[\tau^{xx} h_x^2 + \tau^{zz} - 2h_x \tau^{xz}\right] \left(1 + h_x^2\right)^{-1} = \sigma h_{xx} \left(1 + h_x^2\right)^{-3/2}, \qquad (2.9)$$

where σ is the gas–liquid surface energy and p_{ext} is the external pressure, which need not be constant. Here, we consider a foam in which the gas bubbles are at constant pressure and therefore p_{ext} is a constant P_G. Since the system is pure and isothermal, there are no Marangoni effects from surfactants or temperature-dependent surface tension nor any other forces on the surface. In this case, the surface tangential stress is continuous across the gas–liquid interface and, since the gas is stationary and inviscid, the boundary condition for the liquid film is one of vanishing tangential stress giving

$$\left[\left(h_x^2 - 1\right)\tau^{xz} + h_x(\tau^{xx} - \tau^{zz})\right] = 0. \qquad (2.10)$$

The free film is bisected by a centreline of symmetry at $z = 0$, along which $\tau^{xz} = 0$ and $w = 0$. An effective pressure $p^* = p + \phi$ is used to replace p in the bulk and in the interfacial conditions by $p^* - \phi$.

The analysis proceeds by examining a 'corner' of the liquid region surrounding a gas bubble, representing the smallest repeatable unit that can be used by symmetry operations to generate the entire foam. The 'corner' is divided into three regions, each of which is characterized by different scaling. Figure 1 shows the geometry of the liquid corner configuration. The lamellar region is a thin film within which viscous forces are dominant. The Plateau border region is not a thin film, and therein the capillary forces dominate. To match these two regions an internal transition region is required, which is also a thin film, in which both capillary and viscous forces balance.

This analysis is strictly two-dimensional. Within the given two-dimensional section of the foam, mass balance requires that the total fluid area remains constant, i.e. liquid is not allowed to drain out of the plane of the given cross-sectional area considered. The total length of the domain also remains constant.

2.2. *Viscosity*

It is useful to estimate the magnitude of the shear rate $\dot{\gamma}$ within a free-film of a foam. In lubrication theory applied to a film on a substrate, the speed of the fluid ranges from U to 0 over a distance h, the thickness of the fluid layer. The shear rate is dominated by this variation and so $\dot{\gamma} \sim U/h \sim |u_z|$, where z is the coordinate across the film. In free-films the flow is plug-flow to leading order and in general the flow varies along the film, so that the leading-order shear rate is $\dot{\gamma} \approx |\eta u_x|$, where u is the lateral component of the fluid velocity.

Using estimates from Breward & Howell (2002) and Brush & Davis (2005) for the fluid velocity, the lamellar and the transition region lengths and the (Newtonian) viscosity, it can be shown that in the lamellar region the shear rate $\dot{\gamma} \approx 3\,\mathrm{s}^{-1}$, whereas in the transition region $\dot{\gamma} \approx 3 \times 10^3\,\mathrm{s}^{-1}$. (These examples are for foams consisting of liquid metal or aqueous solution, which have the largest shear rates among the foams that have been studied.) The shear rate in the transition region is much larger than that in the lamella because the length of the transition region is much smaller. It is anticipated that significant variation in the liquid viscosity can be observed during film thinning within the transition region and possibly also within the lamellar region.

Previous work on Newtonian foams shows that at leading order in capillary number, the lateral component of the fluid speed reaches its maximum at the lamellar/transition region boundary and is a minimum at the transition/Plateau

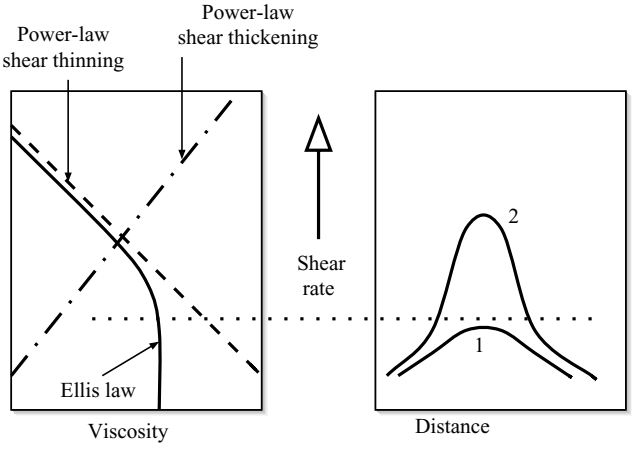

FIGURE 2. Schematic log–log plots of the shear rate versus the viscosity on the left-hand side and the shear rate versus distance in the transition region on the right-hand side. Both the power-law and the Ellis models of the viscosity are shown on the left. The horizontal line indicates the critical value of shear rate derived from the Ellis model beyond which the flow is characterized by power-law behaviour. Curve 1 represents a case in which the viscosity is not large enough for the fluid to exhibit power-law behaviour in the Ellis model, whereas in curve 2 it is large enough. Estimates predict that the shear rate in the transition region in some foams can be much larger than the critical value.

border boundary (Brush & Davis 2005). Therefore, the shear rate vanishes at these boundaries, and the power-law viscosity is unbounded for shear-thinning fluids ($n < 1$) at these locations. Nevertheless, the power law is included in this work, because this model has been used extensively in many studies, data are available for a variety of power-law fluids, the calculated solutions for the shape, the shear rate and the pressure fields within the foam layer are not singular as will be demonstrated later and the solutions reproduce the Newtonian fluid results in the instance $n \to 1$. In addition, the viscosity of shear-thickening fluids is not singular according to the power-law model, in which as $\dot{\gamma} \to 0$ then $\eta \to 0$. Nevertheless, the accuracy of any generalized Newtonian fluid model is always a consideration (Myers 2005), particularly at low shear rates, therefore, the Ellis model is also included in this analysis. The Ellis model viscosity is well behaved at locations where the shear rate vanishes. The results determined from the power law will be compared to those of the Ellis law, providing additional insight. In figure 2 schematic diagrams of the shear rate versus the viscosity and of the shear rate as a function of the distance within the transition region are shown. The figure qualitatively illustrates possible variations of the viscosity within the transition region as a function of the shear rate. However, in an actual foam any changes in the viscosity would not be expected to be symmetric about the midpoint of the (asymmetric) transition region.

3. Analysis

3.1. *Scaling in the Plateau border region*

Dimensionless fluid motion, continuity and energy equations and boundary conditions appropriate for the capillary static region are derived by transforming the equations

according to:

$$\left.\begin{aligned}(\tilde{x},\tilde{z}) &= \left(\frac{x}{L_0},\frac{z}{L_0}\right), \quad (\tilde{u},\tilde{w}) = \left(\frac{u}{U_0},\frac{w}{U_0}\right),\\ \tilde{t} &= \left(\frac{U_0}{L_0}\right)t, \quad \text{and} \quad \tilde{P} = \left(\frac{L_0}{\sigma}\right)p^*,\end{aligned}\right\} \tag{3.1}$$

where L_0 is the initial lamella length, U_0 is a velocity to be determined and σ is the gas–liquid surface tension. There are no body-force potentials in bulk liquid ($\phi = 0$). Additionally, the capillary number $C = \eta_s U_0/\sigma$, where η_s is a particular value of the viscosity which can be provided later if needed. The following dimensionless equations are derived for the bulk liquid:

$$ReC\,(\tilde{u}_{\tilde{t}} + \tilde{u}\tilde{u}_{\tilde{x}} + \tilde{w}\tilde{u}_{\tilde{z}}) = -\tilde{P}_{\tilde{x}} + C\,\{2\,[\tilde{\eta}\tilde{u}_{\tilde{x}}]_{\tilde{x}} + [\tilde{\eta}\,(-\tilde{u}_{\tilde{x}\tilde{x}} + \tilde{u}_{\tilde{z}\tilde{z}})] + \tilde{\eta}_{\tilde{z}}\,[\tilde{w}_{\tilde{x}} + \tilde{u}_{\tilde{z}}]\}, \tag{3.2}$$

$$ReC\,(\tilde{w}_{\tilde{t}} + \tilde{u}\tilde{w}_{\tilde{x}} + \tilde{w}\tilde{w}_{\tilde{z}}) = -\tilde{P}_{\tilde{z}} + C\,\{2\,[\tilde{\eta}\tilde{w}_{\tilde{z}}]_{\tilde{z}} + [\tilde{\eta}\,(-\tilde{w}_{\tilde{z}\tilde{z}} + \tilde{w}_{\tilde{x}\tilde{x}})] + \tilde{\eta}_{\tilde{x}}\,[\tilde{w}_{\tilde{x}} + \tilde{u}_{\tilde{z}}]\}, \tag{3.3}$$

where $\tilde{\eta} = \eta/\eta_s$. The continuity equation is

$$\tilde{u}_{\tilde{x}} + \tilde{w}_{\tilde{z}} = 0. \tag{3.4}$$

At the gas–liquid interface $\tilde{z} = \tilde{h}(\tilde{t},\tilde{x})$,

$$\tilde{w} = \tilde{h}_{\tilde{t}} + \tilde{u}\tilde{h}_{\tilde{x}}, \tag{3.5}$$

$$-\Delta\tilde{P} + \frac{2\tilde{\eta}C}{\left(1+\tilde{h}_{\tilde{x}}^2\right)}\left[\tilde{u}_{\tilde{x}}\tilde{h}_{\tilde{x}}^2 + \tilde{w}_{\tilde{z}} - \tilde{h}_{\tilde{x}}\,(\tilde{u}_{\tilde{z}} + \tilde{w}_{\tilde{x}})\right] = \frac{\tilde{h}_{\tilde{x}\tilde{x}}}{\left(1+\tilde{h}_{\tilde{x}}^2\right)^{3/2}} \tag{3.6}$$

and

$$-2\tilde{\eta}\,(\tilde{u}_{\tilde{x}} - \tilde{w}_{\tilde{z}})\,\tilde{h}_{\tilde{x}} + \tilde{\eta}\,(\tilde{u}_{\tilde{z}} + \tilde{w}_{\tilde{x}})\left(1 - \tilde{h}_{\tilde{x}}^2\right) = 0. \tag{3.7}$$

Finally, at the centreline

$$\tilde{u}_{\tilde{z}} = \tilde{w} = 0. \tag{3.8}$$

Since capillary forces are dominant over viscous effects in the Plateau border then, at leading order in C, the determination of the border shape does not require knowledge of the fluid velocity. Thus, the set of equations governing the shape in a foam with a generalized Newtonian liquid is identical to the set governing the interface shape in a Newtonian liquid foam. The leading-order interface shape in the Plateau border region is

$$\tilde{h}(\tilde{x},\,\cdot) = h_{ol} + \tilde{a}\left(1 - \frac{1}{\sqrt{2}}\right) - \frac{1}{\sqrt{2}\Delta P} + \frac{1}{\Delta P}\left\{1 - \left[\frac{1}{\sqrt{2}} - \Delta P\left(\tilde{x} - L - \frac{\tilde{a}}{\sqrt{2}}\right)\right]^2\right\}^{1/2}, \tag{3.9}$$

where the notation $\tilde{h}(\tilde{x},\cdot)$ refers to a specific instant in time, h_{ol} is an unknown constant, ΔP is the pressure jump across the gas–liquid interface and $\tilde{a}$ is the Plateau border radius of curvature. However, the matching conditions between the Plateau border and the transition region may be different for foam with a non-Newtonian liquid than for foam with a Newtonian liquid. Therefore, the coefficients h_{ol} and ΔP remain undetermined.

3.2. *Derivation of the thin-film equations*

The derivation of the thin free-film models in this study is similar to the derivation used by Erneux & Davis (1993). However, the treatment of the viscous stresses is different and so the details are included below.

The lamellar region is a thin film. Let $\epsilon = h_0/L_0 \ll 1$ be the ratio of the initial lamellar thickness to the initial lamellar length. The scalings appropriate for a thin lamellar region are

$$\left.\begin{aligned} X &= \tfrac{x}{L_0}, \quad Z = \frac{z}{h_0}, \quad T = \frac{U_0}{L_0}t, \quad U = \frac{u}{U_0}, \\ W &= \frac{W}{\epsilon U_0}, \quad P = \frac{\epsilon^2 L_0}{\eta_s U_0}p^* \quad \text{and} \quad H = \frac{h}{h_0}, \end{aligned}\right\} \tag{3.10}$$

where η_s is a viscosity scale, which is chosen later. The components of the stress tensor are scaled by

$$(\hat{\tau}^{XX}, \hat{\tau}^{ZZ}) \equiv \frac{(\tau^{XX}, \tau^{ZZ})}{(\eta_s U_0/L_0)} \quad \text{and} \quad \hat{\tau}^{XZ} \equiv \frac{\tau^{XZ}}{(\eta_s U_0/h_0)}. \tag{3.11}$$

The set of equations governing dynamics within the film are

$$\epsilon^2 Re\,(U_T + UU_X + WU_Z) = -P_X - \hat{\tau}_Z^{ZX} - \epsilon^2 \hat{\tau}_X^{XX}, \tag{3.12}$$

$$\epsilon^4 Re\,(W_T + UW_X + WW_Z) = -P_Z - \epsilon^2 \hat{\tau}_X^{XZ} - \epsilon^2 \hat{\tau}_Z^{ZZ} \tag{3.13}$$

and

$$U_X + W_Z = 0. \tag{3.14}$$

At the gas–liquid interface $Z = H(X, T)$:

$$W = H_T + UH_X, \tag{3.15}$$

$$-P + P_G - \frac{\left[\epsilon^4 H_X^2 \hat{\tau}^{XX} + \epsilon^2 \hat{\tau}^{ZZ} - 2\epsilon^2 H_X \hat{\tau}^{XZ}\right]}{\left(1 + H_X^2\right)} = \frac{\epsilon^3 C^{-1} H_{XX}}{\left(1 + \epsilon^2 H_X^2\right)^{3/2}} \tag{3.16}$$

and

$$\epsilon^2 H_X \left[\hat{\tau}^{XX} - \hat{\tau}^{ZZ}\right] - \hat{\tau}^{XZ}\left(1 - \epsilon^2 H_X^2\right) = 0, \tag{3.17}$$

where P_G is the (uniform) pressure in the gas bubble and $C = \eta_s U_0/\sigma$ is the capillary number. At the free-film centreline ($Z = 0$):

$$U_Z = W = 0. \tag{3.18}$$

In the rescaled variables the components of stress tensor are

$$\hat{\tau}^{XX} = -2\tilde{\eta} U_X, \quad \hat{\tau}^{ZZ} = -2\tilde{\eta} W_Z \quad \text{and} \quad \hat{\tau}^{XZ} = \tilde{\eta}\left(U_Z + \epsilon^2 W_X\right). \tag{3.19}$$

The two models of the viscosity are also rescaled. Substituting the normal components of the stress tensor, the power-law viscosity becomes

$$\tilde{\eta} = K\left\{U_Z^2 + 2\epsilon^2\left[\left(U_X^2 + W_Z^2\right) + W_X U_Z\right] + \epsilon^4 W_X^2\right\}^{(n-1)/2}, \tag{3.20}$$

where $K = kU_0^{n-1}/(\eta_s h_0^{n-1})$. The Ellis viscosity becomes

$$\frac{1}{\tilde{\eta}} = 1 + C_v^{\alpha-1}\left|\left[\frac{1}{2}\left((\hat{\tau}^{XX})^2 + (\hat{\tau}^{ZZ})^2 + \frac{2}{\epsilon^2}(\hat{\tau}^{XZ})^2\right)\right]^{1/2}\right|^{\alpha-1}, \tag{3.21}$$

where $C_v = \eta_0 U_0/|\tau_{1/2}|L_0$. Later the viscosity will be further simplified. (Note that the dimensionless viscosities of both the power-law and Ellis models are denoted by $\tilde{\eta}$; however, the scalings for the two models will not be the same.)

The functions U, W, P, $\hat{\tau}^{XX}$, $\hat{\tau}^{XZ}$ and $\hat{\tau}^{ZZ}$ are expanded as series in even powers of ϵ, i.e. any such function $\phi = \phi^{(0)} + \epsilon^2\,\phi^{(1)} + \cdots$. In the bulk liquid at $O(1)$ in ϵ

$$-P_X^{(0)} - \hat{\tau}_Z^{XZ(0)} = 0, \tag{3.22}$$

$$-P_Z^{(0)} = 0 \tag{3.23}$$

and

$$U_X^{(0)} + W_Z^{(0)} = 0. \tag{3.24}$$

At the gas–liquid interface

$$P^{(0)} = P_G, \tag{3.25}$$

$$\hat{\tau}^{XZ(0)} = 0, \tag{3.26}$$

$$W^{(0)} = H_T + U^{(0)} H_X, \tag{3.27}$$

and, at the centreline

$$W(0) = U_Z^{(0)} = 0. \tag{3.28}$$

Leading-order solutions are: $U^{(0)}(X, T)$ is independent of Z,

$$P^{(0)} = P_G,\ \ \hat{\tau}^{XZ(0)} = 0,\ \ W^{(0)} = -U_X^{(0)} Z \tag{3.29}$$

and, therefore,

$$H_T + \left(U^{(0)} H\right)_X = 0. \tag{3.30}$$

The governing set of equations at $O(\epsilon^2)$ are

$$Re\left(U_T^{(0)} + U^{(0)} U_X^{(0)}\right) = -P_X^{(1)} - \hat{\tau}_X^{XX(0)} - \hat{\tau}_Z^{XZ(1)}, \tag{3.31}$$

$$-P_Z^{(1)} - \hat{\tau}_Z^{ZZ(0)} = 0 \tag{3.32}$$

and

$$U_X^{(1)} + W_Z^{(1)} = 0. \tag{3.33}$$

At the gas–liquid interface $Z = H(X, T)$

$$W^{(1)} = U^{(1)} H_X \tag{3.34}$$

and

$$-P^{(1)} - \hat{\tau}^{ZZ(0)} = \overline{C}^{-1} H_{XX}. \tag{3.35}$$

The capillary number has been rescaled as $\overline{C}^{-1} \equiv \epsilon C^{-1}$ in order to retain capillary effects in the free film. In addition,

$$\left[\hat{\tau}^{XX(0)} - \hat{\tau}^{ZZ(0)}\right] H_X - \hat{\tau}^{XZ(1)} - H_X^2 \hat{\tau}^{XZ(0)} = 0. \tag{3.36}$$

Completing the $O(\epsilon^2)$ set of equations are the conditions at the free-film centreline ($Z = 0$):

$$U_Z^{(1)} = W^{(1)} = 0. \tag{3.37}$$

Solutions to the $O(\epsilon^2)$ system are found first by integrating (3.32) and using (3.35) to discover $P^{(1)} + \hat{\tau}^{ZZ(0)} = -\overline{C}^{-1} H_{XX}$. Differentiating and substituting into (3.31) gives

$$\hat{\tau}^{XZ(1)} = (-Re[U_T^{(0)} + U^{(0)} U_X^{(0)}] + \overline{C}^{-1} H_{XXX} + \hat{\tau}_X^{ZZ(0)} - \hat{\tau}_X^{XX(0)}) Z + C_4(X, T), \tag{3.38}$$

where C_4 is an unknown function. The assumption has been made, consistent with this analysis, that $\hat{\tau}_X^{ZZ(0)}$ and $\hat{\tau}_X^{XX(0)}$ are not functions of Z. Since

$$\hat{\tau}^{XZ} = \tilde{\eta}\left[U_Z + \epsilon^2 W_X\right] = \hat{\tau}^{XZ(0)} + \epsilon^2 \hat{\tau}^{XZ(1)} + \cdots \tag{3.39}$$

and $\hat{\tau}^{XZ(0)} = 0$, it follows that $\hat{\tau}^{XZ(1)} \propto U_Z^{(1)} + W_X^{(0)}$. At $Z = 0$, these derivatives each vanish as required by the $O(1)$ solutions, and by the condition (3.37). Thus, $\hat{\tau}^{XZ(1)}(Z=0) = C_4$ by (3.38), so that $C_4 = 0$. Evaluating $\hat{\tau}^{XZ(1)}$ at the liquid–gas interface and substituting the result into (3.36) gives

$$\left(-Re\left[U_T^{(0)} + U^{(0)}U_X^{(0)}\right] + \overline{C}^{-1}H_{XXX}\right)H + \left[\left(\hat{\tau}^{ZZ(0)} - \hat{\tau}^{XX(0)}\right)H\right]_X = 0. \tag{3.40}$$

Also noting that $\hat{\tau}^{ZZ(0)} \propto W_Z^{(0)}$ and $\hat{\tau}^{XX(0)} \propto U_X^{(0)}$, then from the continuity equation at leading order, $\hat{\tau}^{ZZ(0)} = -\hat{\tau}^{XX(0)}$ and the quantity $\hat{\tau}^{ZZ(0)} - \hat{\tau}^{XX(0)}$ in (3.40) may be replaced by $-2\hat{\tau}^{XX(0)}$. The final result is the pair of coupled equations:

$$Re\left[U_T^{(0)} + U^{(0)}U_X^{(0)}\right]H = \overline{C}^{-1}H_{XXX}H - \left[2\hat{\tau}^{XX(0)}H\right]_X, \tag{3.41}$$

and the leading-order continuity equation, (3.30) (repeated here),

$$H_T + \left(U^{(0)}H\right)_X = 0, \tag{3.42}$$

governing flow and interface shape in the thin film. In the generalized Newtonian liquid free film, the effect of the variable viscosity is included in $\hat{\tau}^{XX(0)}$.

A (leading-order) solution of (3.41) and (3.42) is a uniformly thinning lamella $H_L(T)$ with a fluid velocity $U(X) = \overline{Q}X/L(T)$, where $L(T)$ is the lamellar length, $\overline{Q} = H_L(T)U(L)$ is the fluid flow rate out of the lamella and into the transition region and L is the location of the lamellar–transition region boundary. The flow rate $\overline{Q}$ is determined by a matching condition between the Plateau border shape and the transition region shape arising at the Plateau border/transition region boundary.

In this work it is also assumed there is no drainage out of the plane (along Plateau borders) and, thus, two additional geometrical conditions are imposed on the domain size and area, constraining the evolution of L and a. At leading order (in capillary number) these integrated expressions are (Brush & Davis 2005)

$$\bar{L} - 1 = \frac{a_0}{L_0}(\bar{a} - 1)\tan\psi, \tag{3.43}$$

$$\frac{h_0 L_0}{a_0^2}(H_L\bar{L} - 1) = \frac{1}{2}(1 - \bar{a}^2)(\tan\psi - \psi), \tag{3.44}$$

in dimensionless form, in which the real length of the lamella is $L(t) = L_0\bar{L}(T)$ and the real Plateau border radius of curvature is $a(t) = a_0\bar{a}(T)$. The subscript '0' denotes the initial value of a parameter. As discussed in Brush & Davis (2005), there are two geometric ratios a_0/L_0 and h_0L_0/a_0^2 either of which can be chosen to be unity leading to different leading-order dynamical results. If $a_0/L_0 \sim 1$ the foam is of 'semi-arid' type in which case $h_0L_0/a_0^2 \sim \epsilon/\delta_0$. In this case, $\overline{a} = \overline{L} = 1$ for all time. If $h_0L_0/a_0^2 \sim 1$, then $a_0/L_0 \sim (\epsilon/\delta_0)^2$, the foam is 'arid'; although $\overline{L} = 1$ for all time, now $\overline{a}$ is a function of the lamellar thickness. In order to complete the analysis, specific forms for the viscosity are derived.

3.3. *Scaling in the transition region*

In order to bring viscous and capillary forces into balance in the transition region, the axial coordinate is stretched according to

$$\hat{X} = \frac{X - L}{\delta}, \tag{3.45}$$

which holds at any instant in time, where $\epsilon \ll \delta \ll 1$ and in which all variables have been scaled by L_0. Despite the coordinate transformation the transition region remains a thin free-film. Applying the transformation to the thin film, continuity equation (3.42) gives

$$H_T - \left[\frac{L_T}{\delta} + \frac{\delta_T \hat{X}}{\delta}\right] H_{\hat{X}} + \frac{\left(U^{(0)}H\right)_{\hat{X}}}{\delta} = 0. \tag{3.46}$$

The leading-order result gives a constant flow rate through the transition region $\overline{Q} \equiv U^{(0)}H$, since all terms involving time derivatives are of higher order. Therefore, for small Re, the transformed equation of motion (3.41) reduces to

$$\overline{C}^{-1} H_{\hat{X}\hat{X}\hat{X}} H \left(\frac{1}{\delta^3}\right) - 2(\hat{\tau}^{0\hat{X}\hat{X}} H)_{\hat{X}} \left(\frac{1}{\delta}\right) = 0. \tag{3.47}$$

The component of the shear stress is proportional to the derivative of the lateral component of the fluid velocity, i.e. $\hat{\tau}^{0\hat{X}\hat{X}} = -2\tilde{\eta} U_X^{(0)} \sim O(1/\delta)$. In order for the viscous forces to balance the capillary-induced-pressure forces at leading order $\hat{C}^{-1} \equiv \overline{C}^{-1}/\delta_0 \sim O(1)$, where $\delta \equiv \bar{\delta}\delta_0$ and $\bar{\delta} \sim O(1)$. Assuming that $\hat{C}^{-1} \sim O(1)$, then without loss of generality $\hat{C}^{-1}$ is set to unity. Equation (3.47) becomes

$$\frac{1}{\delta} H_{\hat{X}\hat{X}\hat{X}} H + 4\left(\tilde{\eta} U_{\hat{X}}^{(0)} H\right)_{\hat{X}} = 0. \tag{3.48}$$

The asymptotic form of the transition region shape at the transition/Plateau border is derived in Appendix A. The result gives the approximate shape of the transition region at the transition region/Plateau border boundary as

$$H = \left(\frac{8\widehat{Q}}{3H_L^{3/2}}\right)^2 \left[\frac{\tilde{\eta}_{-\infty}^2}{2} + D\right] \frac{\hat{X}^2}{2} + A_1 \hat{X} + A_2, \tag{3.49}$$

where $\widehat{Q} = \overline{Q\delta}$,

$$D = \lim_{\hat{X}\to\infty} \left[\tilde{\eta}_{-\infty} \left(\int^{\hat{X}} \tilde{\eta}_{\hat{X}'} \left[\frac{H_L}{H}\right]^{3/2} \mathrm{d}\hat{X}'\right) + \frac{1}{2}\left(\int^{\hat{X}} \tilde{\eta}_{\hat{X}'} \left[\frac{H_L}{H}\right]^{3/2} \mathrm{d}\hat{X}'\right)^2\right], \tag{3.50}$$

$\tilde{\eta}_{\hat{X}'}$ is the derivative of the viscosity with respect to distance in the transition region, $\tilde{\eta}_{-\infty}$ is the scaled viscosity at the lamella/transition border and H_L is the lamellar thickness. The result reveals that, through D, the variable viscosity contributes to the magnitude of the curvature at the transition Plateau border boundary at leading order.

3.4. *Matching*

In order to determine the flow rate $\widehat{Q}$ that governs the thinning rate of a lamella, the transition-region solution (3.49) must be matched to the Plateau-border solution (3.9). Although previously Breward & Howell (2002) and Brush & Davis (2005)

have presented the results of matching procedures in foams, here a systematic and somewhat different analysis is presented in detail in Appendix B. The result is

$$\frac{1}{\epsilon\tilde{a}} = \left(\frac{8\widehat{Q}}{3H_L^{3/2}}\right)^2 \left[\frac{\tilde{\eta}_{-\infty}^2}{2} + D\right] \frac{1}{\delta^2}, \tag{3.51}$$

which is the matching condition for the curvatures of the transition and the Plateau border regions at leading order. In general, $\tilde{a} = a'/L_0$, and $\delta = \delta'/L_0$ may be functions of time, where the 'prime' denotes the dimensional length. Recalling that $\widehat{Q} = \overline{Q\delta}$, $\overline{a} = a'/a_0$, $\overline{\delta} = \delta'/\delta_0$, defining $\breve{Q} \equiv \overline{Q}\sqrt{\tilde{\eta}_{-\infty}^2 + 2D}$, and substituting all quantities in (3.51) gives

$$\frac{\delta_0'^2}{h_0 a_0} = \frac{1}{2}\left(\frac{8\breve{Q}}{3H_L^{3/2}}\right)^2 \overline{a}. \tag{3.52}$$

The above relationship denotes that the left-hand side is constant and the right-hand side is a function of time. Therefore, without loss of generality, both sides are set to unity resulting in

$$\delta_0'^2 = h_0 a_0 \quad \text{and} \quad \breve{Q} = \frac{3\sqrt{2}}{8}\frac{H_L^{3/2}}{\overline{a}^{1/2}}. \tag{3.53}$$

The first condition in (3.53) represents a balance between capillary forces of the Plateau border and the pressure forces in the transition region. This balance of forces couples with the additional previously imposed balance between the capillary induced pressure forces and the viscous forces in the transition region, i.e. $C = \epsilon/\delta_0$, to set the lateral fluid velocity scale, namely, $U_0 = \sigma/\eta_s\sqrt{h_0/a_0}$. The second matching condition relates the flow rate $\breve{Q}$ to the scaled radius of curvature of the Plateau border and the scaled thickness of the lamella. However, $\breve{Q}$ depends on the parameter D, which involves the integration of a function of the transition-region shape over the entire transition region. Thus, although constant, D introduces a non-local contribution to the matching condition. This is a fundamental difference between the non-Newtonian and the Newtonian liquid. Therefore, the solution to the equations governing the shape and the viscosity in the transition region, which matches with the Plateau border and the lamella appropriately, is determined by the numerical procedure described below. In the Newtonian limit the matching results reduce exactly to the form given in Brush & Davis (2005).

3.5. *Numerical evaluation*

The transition-region shape obeys the quasi-static equation:

$$\frac{\epsilon C^{-1}}{\delta} H_{\hat{X}\hat{X}\hat{X}} H - 4\overline{Q}\left(\tilde{\eta} H_{\hat{X}} H\right)_{\hat{X}} = 0, \tag{3.54}$$

because the flow rate $\overline{Q} \equiv UH$ is constant throughout the transition region at any instant in time. The transformed interface shape $H = FH_L$ is introduced so that at the lamellar-transition boundary,

$$F \equiv \frac{H}{H_L} \to 1 \quad \text{as} \quad X \to -\infty. \tag{3.55}$$

At the transition–Plateau border the leading-order curvatures are matched giving

$$F_{XX} \to 1 \text{ as } \hat{X} \to \infty, \text{ provided that } \overline{\delta} = (H_L\overline{a})^{1/2}, \tag{3.56}$$

which requires that $\delta' = (h_L a')^{1/2}$ in dimensional form. The equation governing the transition-region shape is then

$$\frac{H_L^2}{\overline{\delta}} F_{\hat{X}\hat{X}\hat{X}} F - 4\overline{Q}\left(\tilde{\eta}\frac{F_{\hat{X}}}{F}\right)_{\hat{X}} = 0, \tag{3.57}$$

since $\epsilon C^{-1}/\delta_0 = 1$. Once again these scalings give the characteristic fluid velocity

$$U_0 = \frac{\sigma}{\eta_s}\left(\frac{h_0}{a_0}\right)^{1/2}, \tag{3.58}$$

where η_s is given below. In a Newtonian fluid the scaled viscosity $\tilde{\eta}$ is unity and the coefficients in (3.57) must balance to give $\overline{Q}\overline{\delta}/H_L^2 \sim O(1)$, so that $\overline{Q} \sim H_L^{3/2}/\overline{a}^{1/2}$. In the case of a generalized Newtonian fluid the same balance applies; however, the ratio of the two coefficients will be a function of the material viscosity parameters. The two viscosity models are examined below.

3.5.1. *Power-law foam*

The power-law viscosity is written in terms of the components of the fluid velocity:

$$\tilde{\eta} = K\left\{U_Z^2 + 2\epsilon^2\left[\left(U_X^2 + W_Z^2\right) + W_X U_Z\right] + \epsilon^4 W_X^2\right\}^{(n-1)/2}, \tag{3.59}$$

where $K = kU_0^{n-1}/(\eta_s h_0^{n-1})$, $\tilde{\eta} \equiv \eta/\eta_s$, and η_s is a scale factor to be chosen. The fluid velocities are expanded in even powers of ϵ, and since the flow is lateral, the leading-order term in the expansion of $U(X, Z, T)$ is not a function of Z, i.e. $U^{(0)}(X, T)$. Therefore, the coefficient K must be rescaled as $\overline{K} = \epsilon^{n-1}K$. Proceeding with the expansion of the viscosity the leading-order result is

$$\tilde{\eta} = 2^{n-1}\overline{K}\left|U_X^{(0)}\right|^{n-1}. \tag{3.60}$$

In the transition region,

$$U_{\hat{X}}^{(0)} = \frac{-\overline{Q}H_{\hat{X}}}{H^2}, \tag{3.61}$$

after transforming to transition region coordinates. It follows that

$$\tilde{\eta} = \frac{2^{n-1}\overline{K}\,\overline{Q}^{n-1}}{\delta^{n-1}H_L^{n-1}}\left|\frac{F_{\hat{X}}}{F^2}\right|^{n-1}. \tag{3.62}$$

The equation for the shape of the transition region (3.57) is integrated once, and the expression for the viscosity (3.62) is substituted into the result giving

$$F_{\hat{X}\hat{X}} = \frac{(F_{\hat{X}})^2}{2F} + 4\lambda^n\left|\frac{F_{\hat{X}}}{F^2}\right|^{n-1}\frac{F_{\hat{X}}}{F^2}, \tag{3.63}$$

where

$$\lambda^n = \frac{2^{n-1}\overline{Q}^n\overline{K}}{H_L^{n+1}\overline{\delta}^{n-2}\delta_0^{n-1}}. \tag{3.64}$$

Note that for fixed n, λ is a constant. By choosing the viscosity scale to be

$$\eta_s = \frac{kU_0^{n-1}}{(a_0' h_0)^{(n-1)/2}}, \tag{3.65}$$

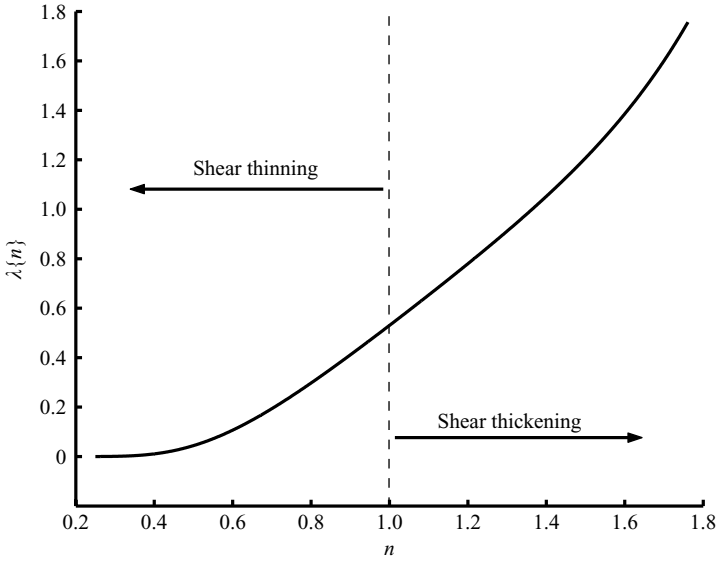

FIGURE 3. The function $\lambda\{n\}$ versus the power-law exponent n. The value $\lambda\{1\} = 0.5303$ represents a Newtonian liquid, whereas $n < 1$ is shear thinning and $n > 1$ is shear thickening.

the flow rate becomes

$$\overline{Q} = \left(\frac{\lambda}{2^{1-1/n}}\right) H_L^{3/2} \overline{a}^{1/2-1/n}, \tag{3.66}$$

so that the equation for lamellar thinning becomes

$$\frac{\mathrm{d}H_L}{\mathrm{d}T} = -\left(\frac{\lambda}{2^{1-1/n}}\right) H_L^{3/2} \overline{a}^{1/2-1/n}. \tag{3.67}$$

The derived scalings are summarized:

$$U_0 = \left(\frac{\sigma}{ka_0'}\right)^{1/n} \sqrt{a_0' h_0} = \left(\frac{\sigma}{ka_0'}\right)^{1/n} \delta_0', \tag{3.68}$$

$$\eta_s = \frac{\sigma}{a_0'} \left[\frac{\sigma}{ka_0'}\right]^{-1/n}, \tag{3.69}$$

and the time scale, L_0/U_0, is

$$\tau = \left(\frac{\sigma}{ka_0'}\right)^{-1/n} \frac{1}{\delta_0} \tag{3.70}$$

recalling that $\delta_0 = \delta_0'/L_0$.

The function $\lambda\{n\}$ is determined by the numerical solution of (3.63) subject to the end conditions, (3.55) and (3.56). The numerical method sets the value of the transition region thickness as well as an initial value of the interface slope at $X = 0$, and then iterates the slope until convergence of the solution to both of the end conditions, using a two-directional shooting method. The values of $\lambda\{n\}$ are plotted in figure 3 as a function of n; $n < 1$, $n = 1$ and $n > 1$ correspond to shear-thinning, Newtonian and shear-thickening fluids, respectively.

Finally, the loop is closed with regard to the matching procedure presented earlier by equating the flow rates from (3.53) and (3.66), which leads to a relation between λ

and the integral D:

$$\lambda = \frac{3\left(2^{-3/2-1/n}\right)}{\overline{a}^{1-1/n}\sqrt{\tilde{\eta}_{-\infty}^2 + 2D}}. \tag{3.71}$$

For the semi-arid foam, the radius of curvature of the Plateau border remains unchanged during lamellar thinning, i.e. $\overline{a} = 1$. Integration of (3.67) gives the lamellar thickness as a function of time:

$$H_L = \left(1 + \frac{\tilde{T}}{2}\right)^{-2}, \tag{3.72}$$

where the rescaled time is

$$\tilde{T} = T\frac{\lambda}{2^{(1-1/n)}} = \frac{\lambda}{2^{(1-1/n)}}\left(\frac{\sigma}{ka_0'}\right)^{1/n}\frac{(a_0'h_0)^{1/2}}{L_0}t. \tag{3.73}$$

The physical implication of this result is that in a semi-arid foam, the thinning of a liquid lamella with power-law viscosity is identical to the thinning of a liquid Newtonian lamella, but on a reduced time-scale which is calculated here. The time constant is uniquely determined by knowledge of the power-law exponent n (through $\lambda\{n\}$) and the coefficient k for the particular foam liquid phase, giving the characteristic thinning time.

The arid foam may also be integrated after substituting the expression $\overline{a}$ as a function of H_L derived from (3.44) giving

$$\begin{aligned}
&\frac{1}{H_L^{1/2}}\left[\left(\frac{1+R'-H_L}{R'}\right)^{-(n-2)/4n} \times \left(\frac{1+R'-H_L}{1+R'}\right)^{(n-2)/4n}\right. \\
&\quad \left. \times {}_2F_1\left\{-\frac{1}{2}, \frac{n-2}{4n}; \frac{1}{2}; \frac{H_L}{1+R'}\right\}\right] \\
&= \frac{\tilde{T}}{2} + \left(\frac{R'}{1+R'}\right)^{(n-2)/4n} \times {}_2F_1\left\{-\frac{1}{2}, \frac{n-2}{4n}; \frac{1}{2}; \frac{1}{1+R'}\right\}.
\end{aligned} \tag{3.74}$$

Here ${}_2F_1\{a, b; c; x\}$ is the symbol for the hypergeometric function and $R' = (\tan\psi - \psi)/2 > 0$. In the arid foam, as opposed to the semi-arid foam, the difference between Newtonian ($n = 1$) and non-Newtonian foam is not accounted for by a simple rescaling of time, since n appears explicitly in the dynamical equation for the interface thickness.

Table 1 provides the values of k and n for a number of different fluids. The values of k and n for shear-thinning fluids are given by Bird *et al.* (1977) and by Myers (2005). A hypothetical dilatant (shear-thickening fluid) is also given. References for other data are included in the table. The values $h_0 = 10^{-5}$ cm, $L_0 = 10^{-3}$ cm and $a_0 = 10^{-3}$ cm are chosen, valid for semi-arid foam. Hec 0.5% is an aqueous solution containing 0.5% hydroxyethylcellulose. Note that although polystyrene is very slow thinning, it is included in the analysis.

In figure 4 lamellar thicknesses are plotted as a function of time for semi-arid foams and for arid foams having different power-law exponents. In order to compare the different cases, the equations have been re-written in a canonical form by applying the transformations:

$$\hat{h}_L = \frac{2H_L}{(R+2)} \quad \text{and} \quad \hat{t} = \frac{T\lambda\{n\}(R+2)^{1/2}}{2^{3/2-1/n}}, \tag{3.75}$$

Fluid	k (gm s^{n-2} cm^{-1})	n	σ (gm s^{-2})	λ	τ^{-1} (s^{-1})
Hec 0.5%	0.84	0.5088	0.073[a]	0.048	60.66
Blood	0.035	0.6	0.056[b]	0.107	4573.00
Polystyrene	3.5 (10^5)	0.039	0.031[c]	0.009	~0.00
Dilatant	1.0	1.25	0.05[d]	0.811	3.62

[a]Surface tension of water at 20°C.
[b]From Hrncir & Rosin (1997).
[c]From Hamdorf & Johannsmann (2000).
[d]Fictitious material in which the surface tension is chosen to be similar to the other cases.

TABLE 1. Parameters k and n for power-law fluids, their gas–liquid surface energies, the value of λ calculated numerically from the solution to (3.63), and the characteristic time scale for thinning given in (3.73). The viscosity parameters, except for the dilatant liquid, were taken from Myers (2005) and from Bird *et al.* (1977).

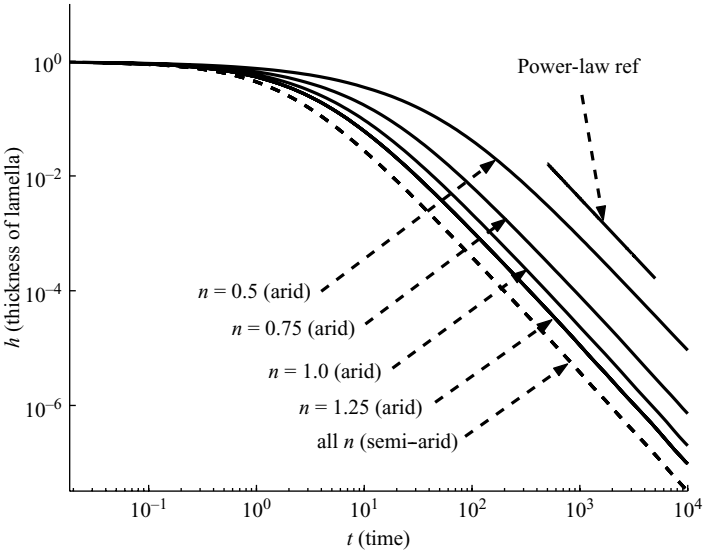

FIGURE 4. Plot of the lamellar thickness as a function of time for semi-arid (dashed line) and arid (solid lines) foams and for different power-law exponents, $n = 0.5$, 0.75, 1.0 and 1.25. The time scale has been chosen so that the semi-arid foam is independent of n in these coordinates; however, the arid foam is not. In the arid case, as the viscosity power-law exponent becomes larger, the thinning rate increases. Of course, the actual evolution of the film thickness in dimensional time depends on the parameter k in the power-law fluid.

where $R = \tan\psi - \psi > 0$, which is slightly different from the form written in Brush & Davis (2005). The semi-arid thinning rate is given by

$$\frac{\mathrm{d}\hat{h}_L}{\mathrm{d}\hat{t}} = -\hat{h}_L^{3/2}. \tag{3.76}$$

The arid thinning rate is given by

$$\left(\frac{1}{p}\right)\frac{\mathrm{d}\hat{h}_L}{\mathrm{d}\hat{t}} = -\hat{h}_L^{3/2}\left[1-\hat{h}_L\right]^{1/4-1/(2n)} \quad \text{where} \quad p = \left(1+\frac{2}{R}\right)^{1/4-1/(2n)}. \tag{3.77}$$

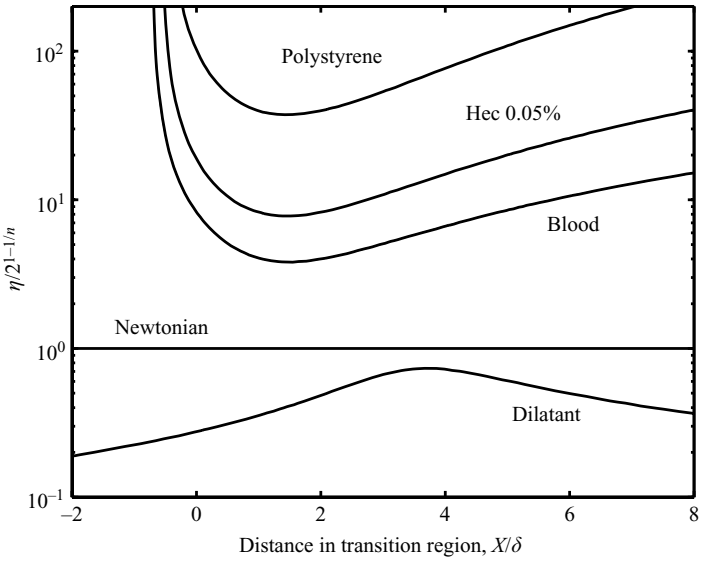

FIGURE 5. The viscosity through the transition region of a number of the liquids listed in table 1. Note that the ordinate $\eta/2^{1-1/n}$ is equal to $\lambda|F_X/F^2|^{n-1}$.

The results presented in figure 4 show that in all cases, after an initial transient, the lamellae settle into a t^{-2} power-law thinning behaviour. In these variables, as discussed previously, there is only one thinning law for all semi-arid foams, given by the solution of (3.76). This result is consistent with the conclusions reached by Safouane *et al.* (2006) based on observations from their forced foam drainage experiments. They concluded that there is a particular effective viscosity for foams with shear-thinning liquid, for which the drainage of liquid from the foam (into a liquid reservoir) occurs at the same rate (obeys the same law) as would the drainage of liquid from a foam consisting of a Newtonian liquid of the same effective viscosity. Although a change in time scale could be made for arid foam that would eliminate the coefficient p in (3.77), no transformation can eliminate the explicit dependence of the thinning rate equation on the power-law exponent n. Therefore, an invariant dynamical law cannot be found for the thinning of lamellae in arid foams. Finally, figure 4 also shows that the properties of the fluid primarily affect only the initial transient during thinning as all foams eventually evolve into identical power-law behaviour. However, in the cases shown, the transient stage can account for nearly a century of lamellar thinning.

Figure 5 shows plots, on a logarithmic scale, of the viscosity $\tilde{\eta}/2^{1-1/n}$ within the transition region for foams that consist of the liquids listed in table 1. Blood, hydroxyethylcellulose and polystyrene are shear thinning and all viscosities exhibit singular behaviour at the boundaries of the transition region where the shear rate vanishes. Examples of a fictitious dilatant (shear thickening) liquid foam and Newtonian liquid foam are also given, both exhibiting well-behaved viscosities. In all of the numerical calculations, the transition-region height is assigned the value 1.01 at the location $\hat{X}=0$, so that the heights of calculated transition regions are all identical at this location. The results show that the shear-thinning fluids blood, hydroxyethylcellulose and polystyrene have minima in viscosity at $\hat{X}=1.49$, 1.46 and 1.49, respectively, despite the wide range in magnitude of the transition region viscosities for these materials. Note, however, that the shear-thickening foam has an

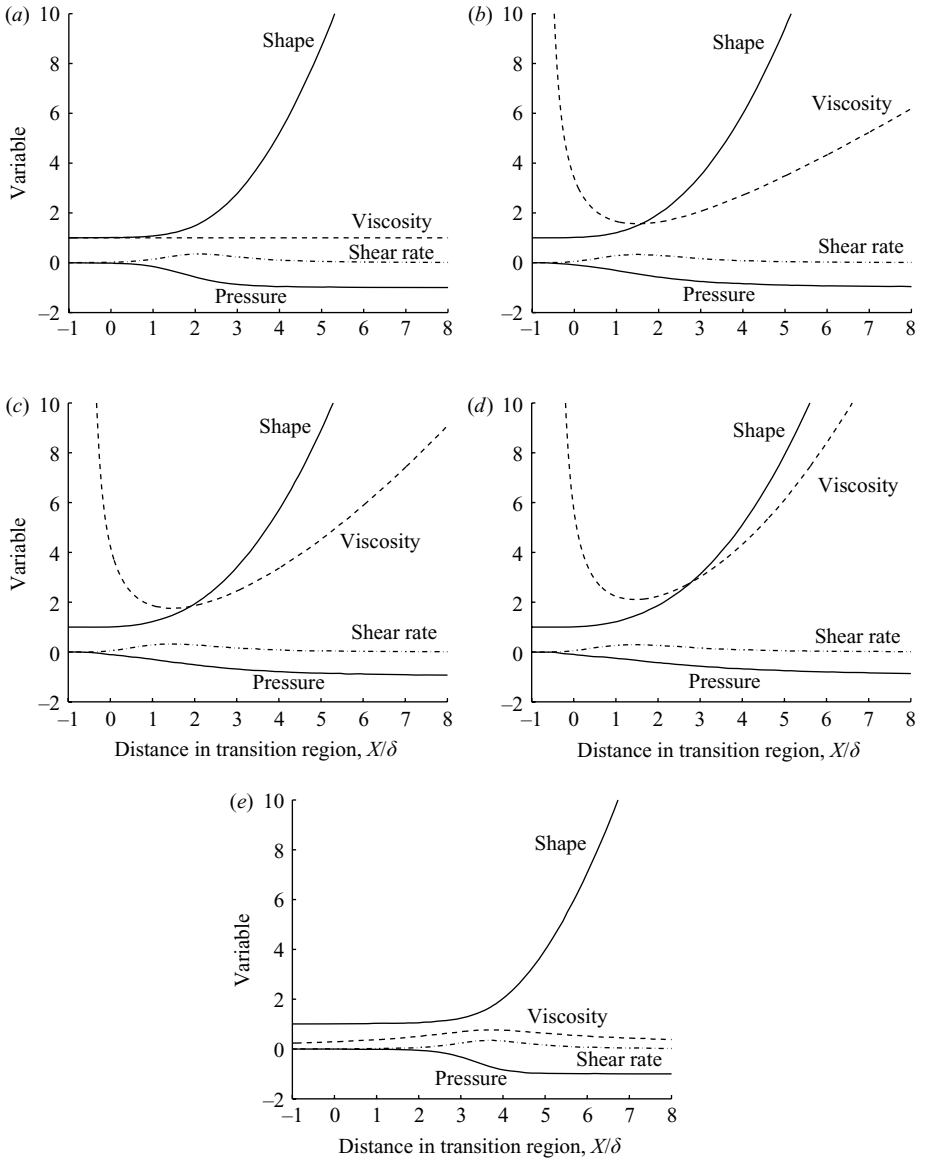

FIGURE 6. Transition region functions for (*a*) Newtonian Al, (*b*) blood, (*c*) hydroxyethylcellulose, (*d*) polystyrene and (*e*) a hypothetical shear-thickening liquid, generated with a power-law model of the viscosity.

extrema in viscosity further away from the lamellar-transition border than do the other cases.

In figure 6 the transition-region shape F, and measures of the viscosity, $\tilde{\eta}/2^{1-1/n}$, the pressure, $P\delta_0$, and the shear rate, $2^{1/2-1/n}|\dot{\gamma}|/(\sigma/ka_0')^{1/n}$, are plotted for the same foams as presented in figure 5. Despite the singular nature of the viscosity at the transition-region boundaries, the values of all other functions in the transition region are well behaved. Recall that because of the scaling used for the differential equations governing the interface shape and the viscosity in semi-arid foam, the quantities

plotted in figure 6 are time invariant. In arid foam this is not the case. In all plots shown in figure 6 the ordinates and abscissae are identical, therefore, differences in the viscosity and slight displacements of the shape and the pressure distributions among the shear-thinning and Newtonian cases (figure 6*a–d*) are discernible. However, again, the shear-thickening liquid phase in figure 6(*e*) shows substantial differences in shape and pressure distribution when compared to the other cases.

In order to ascertain the effect of the singularity in the power-law model of the viscosity of shear-thinning liquid foams on the accuracy of the results, in the next section we develop the Ellis model in which the viscosity is well behaved at all shear rates. The results calculated using the Ellis law are compared to those calculated using the power-law viscosity.

3.5.2. *Ellis foam*

Methodology similar to that used in treating the power-law foams is used to derive the lamellar thinning rate and the transition region variables in an Ellis law foam. The viscosity in the Ellis law model is scaled by η_0, which is most appropriate for cases in which the viscosity does not decrease significantly far into the power-law regime (see figure 2). (As will be shown, a more appropriate choice can be made for the case of a highly shear-thinning liquid, such as hydroxyethylcellulose.) All other scalings used in the case of the power-law viscosity foam are retained. This leads to the lamellar thinning rate,

$$\frac{\mathrm{d}H_L}{\mathrm{d}T} = -\overline{Q}, \tag{3.78}$$

where

$$\overline{Q} = \lambda_e \frac{H_L^{3/2}}{\overline{a}^{1/2}}. \tag{3.79}$$

The function λ_e is found from the solution to the coupled equations for the transition region shape,

$$F_{\hat{X}\hat{X}} = \frac{F_{\hat{X}}^2}{2F} + 4\lambda_e \left(\tilde{\eta}\frac{F_{\hat{X}}}{F^2}\right) \tag{3.80}$$

and the viscosity,

$$\frac{1}{\tilde{\eta}^{\alpha}} = \frac{1}{\tilde{\eta}^{\alpha-1}} + \left[\frac{2\sigma\lambda_e}{a_0'|\tau_{1/2}|}\right]^{\alpha-1} \left(\frac{1}{\overline{a}}\frac{|F_{\hat{X}}|}{|F^2|}\right)^{\alpha-1}, \tag{3.81}$$

where $\tilde{\eta} = \eta/\eta_0$. The auxiliary conditions for the shape at the endpoints of the transition region are

$$F_{\hat{X}\hat{X}} \to 1 \qquad \text{as } \hat{X} \to \infty \tag{3.82}$$

and

$$F \to 1 \qquad \text{as } \hat{X} \to -\infty. \tag{3.83}$$

The coefficient λ_e is no longer a simple function of the viscous model parameters because the coupling of the equation of motion with the viscosity is more complex. At any given time the solution to (3.80) and (3.81) is determined by a numerical method similar to that used for the power-law foam model.

The transition-region variables plotted in figure 7 are the shape, and measures of the viscosity, the pressure and the shear rate, scaled for the two materials. The computed value of λ_e is 194 for hydroxyethylcellulose and 0.532 for polystyrene. These two cases represent liquids with vastly different viscous behaviour. (As shown in table 1,

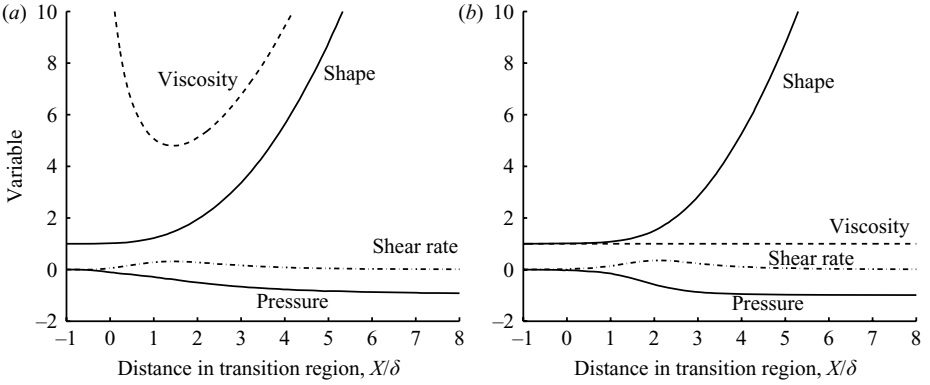

FIGURE 7. (*a*) Transition region variables for hydroxyethylcellulose using the Ellis law in which $Cr = 2961.5$, $\alpha = 2.073$ and λ (computed) = 194. The curves are denoted by (i) 'shape', F, the transition-region shape scaled by the lamellar thickness, (ii) 'viscosity', the actual viscosity scaled by $\eta_0|\tau_{1/2}a_0'/\sigma|^{\alpha-1}$, (iii) 'shear rate', the shear rate scaled by $2^{1/n-1/2}(\sigma/(ka_0'))^{1/n}$, and (iv) 'pressure', the pressure scaled by σ/a_0'. (*b*) Transition-region variables for polystyrene using the Ellis law in which $Cr = 0.049206$, $\alpha = 3.2$ and λ_e (computed) $= 0.531$. The curves are denoted by (i) 'shape', F, (ii) 'viscosity', the actual viscosity scaled by η_0 the viscosity at zero shear rate, (iii) 'shear rate', the shear rate scaled by $2^{1/n-1/2}\lambda_e(\sigma/(ka_0'))^{1/n}$ and (iv) 'pressure', σ/a_0'.

polystyrene has a very large viscosity. Nevertheless, thinning still occurs, although the characteristic time scale is orders of magnitude larger than for hydroxyethylcellulose.) The variable Cr $(= 2\sigma/(|\tau_{1/2}|a_0')$ is an indicator of the tendency of the liquid in a *foam* to exhibit shear-thinning behaviour in the Ellis model. For hydroxyethylcellulose, $Cr = 2961.5$ indicating that in this foam the power-law regime will be predominant in the transition region. The large value of Cr also indicates that if the viscosity is scaled by its value at zero shear rate η_0, it will decrease from unity to nearly zero over a very short distance from the lamellar border just inside the transition region. A more appropriate scaling is given in the caption of figure 7. As shown in figure 7(*a*), the viscosity behaves similar to the power-law case in the interior of the transition region. Near the boundaries of the transition region, the shear rate decreases to zero, so that the Ellis model of the viscosity in the transition region is capped by its value η_0 and is not singular, although this is not shown in the plot. For polystyrene, however, $Cr = 0.492$, which indicates that the liquid will remain Newtonian-like in a foam with a Plateau border radius of curvature of 10^{-5} m. Therefore, in figure 7(*b*) the scale η_0 for the viscosity is retained, and the viscosity is very close to unity throughout the transition region. Finally, if the results calculated for the semi-arid and arid foams using the power-law model of viscosity are superposed on the Ellis model plots shown in figure 7, the shape, the pressure and the shear rates are very difficult to distinguish by eye. The viscosity differs at its minimum by a factor of about 2–3 because of the scalings chosen.

A comparison of semi-arid lamellar thinning rates in hydroxyethylcellulose and polystyrene power-law and Ellis liquid viscosity models provides insight into viscosity model accuracy. The power-law and the Ellis law viscosity parameters for hydroxyethylcellulose and for polystyrene given in table 1 of this work and described in figure 1 of Myers (2005) were determined by matching the power-law and Ellis viscosities in the power-law regime. As a result, at a shear rate in which the Ellis-law behaves as a Newtonian fluid the Ellis fluid will have a lower viscosity than the

power-law fluid. Therefore, in the case of these two liquids, the Ellis lamellar films will thin more rapidly than the power-law films. This is true in all calculations that we performed. However, the disparity between the thinning rates in power-law and Ellis model liquid lamella is not as drastic in the case of hydroxyethylcellulose as in the case of polystyrene, since in the former case most of the transition region is operating in the power-law regime. However, in the case of polystyrene, the shear rate is so low throughout the transition region that the Ellis model behaves as a Newtonian fluid. This is verified by the fact that the numerically determined coefficient λ_e derived for the Ellis model has the value 0.53 which is the value appropriate for a Newtonian lamella in the scaled variables. Moreover, since the shear rate is so low in the case of polystyrene, the disparity between the viscosities of the two models is so large that the power-law model shows an effectively zero thinning rate. The large disparity between the polystyrene power-law and Ellis model results illustrates how a model of the viscosity can be highly inaccurate, although in many cases it may not be obvious which is the more accurate model without experimental observations for validation.

In the power-law foam, the choices used for the velocity and the viscosity scales result in $O(1)$ minimum viscosity, occurring in the interior of the transition region, as can be seen from figures 5 and 6. In the Ellis model, since there are the two viscosity regimes, a different scaling choice may be appropriate if the value of $Cr = 2\sigma/|\tau_{1/2}|a_0'$ is very large. Substituting $\lambda_e = \hat{\lambda}\lambda_s$ and $\eta_e = \hat{\eta}\eta_s$ in (3.80) and (3.81), and for the case in which the viscosity within the transition region becomes very small, the appropriate balancing of terms in the two equations gives

$$\eta_s = \left| \frac{a_0' |\tau_{1/2}|}{2\sigma} \right|^{\alpha-1} \quad \text{and} \quad \lambda_s = \frac{1}{\eta_s}. \tag{3.84}$$

An estimate of the new liquid viscosity scale is found using data for hydroxytheylcellulose, provided in table 1. Assuming that the radius of curvature of the foam Plateau border is 10^{-5} m then $\eta_s = 1.88 \times 10^{-4}\,\mathrm{kg\,(m\,s)^{-1}}$. We identify (3.84) as the appropriate high shear-thinning scale, whereas η_0 would remain as the low shear-thinning scale in foams.

For highly shear-thinning liquids the resulting Ellis foam transition region model becomes

$$F_{\hat{X}\hat{X}} = \frac{F_{\hat{X}}^2}{2F} + 4\hat{\lambda}\left(\hat{\eta}\frac{F_{\hat{X}}}{F^2}\right) \tag{3.85}$$

and

$$\frac{1}{\hat{\eta}^\alpha} = \frac{1}{\hat{\eta}^{\alpha-1}}\left[\frac{2\sigma}{a_0'|\tau_{1/2}|}\right]^{\alpha-1} + \hat{\lambda}^{\alpha-1}\left(\frac{1}{\bar{a}}\frac{|F_{\hat{X}}|}{|F^2|}\right)^{\alpha-1}. \tag{3.86}$$

However, the functional form of the lamellar thinning rate remains invariant:

$$\frac{\mathrm{d}H_L}{\mathrm{d}\bar{T}} = -\hat{\lambda}\frac{H_L^{3/2}}{\bar{a}^{1/2}}. \tag{3.87}$$

provided that time is rescaled by $\bar{T} = T\lambda_s$.

4. Discussion

The analysis of the problem of the thinning of lamella in a non-Newtonian foam can be stated as a flow problem in which the essential parameters that describe the

geometry of the foam are time dependent and the viscosity varies along the direction of flow (a contrast with the work of Myers 2005.) Despite these complexities progress can be made in identifying an apparent viscosity which can be used in the canonical equations developed in Brush & Davis (2005).

The aim is to take two descriptions of the fluid viscosity and equate them in such a way that their dimensional time scales for thinning are the same. In this way the material parameters that describe an Ellis fluid can be converted to apparent material parameters for either a power-law fluid or a Newtonian fluid, so that the simplicity of these latter models can be exploited in calculations. Such a condition will result in a relationship between the functions λ_e calculated in the Ellis model and with $\lambda\{n\}$ calculated in the power-law model. Also setting the interface thickness scales equal, the following identity is derived

$$\frac{2^{1-1/n}k^{2/n}\sigma^{1-2/n}}{(a_0')^{2-2/n}\eta_0}\hat{\lambda}_e = \lambda\{n\}. \tag{4.1}$$

This result guarantees that the canonical form of the semi-arid Ellis and power-law models provide identical real-time thinning rates. If all of the model parameters are known, then (4.1) gives λ_e in terms of $\lambda\{n\}$. Alternatively, suppose α is unknown. Then, given an initial guess for α, the results for the Ellis model can be iterated using (4.1) until the appropriate value of α is found bringing the thinning rates into agreement.

The results of this analysis support the suggestion by Myers (2005) that predictions of the fluid velocity using the power-law model may be inaccurate. For the hydroxyethylcellulose solution figures 6(c) and 7(a) show very similar flows, whereas for polystyrene figures 6(d) and 7(b) show significant differences. In the former case, the shear rate in the transition region is sufficiently high that according to the Ellis model the fluid exhibits mostly power-law behaviour. In the latter case, the shear rate is so low that the fluid will be primarily Newtonian and according to the Ellis model which accounts for low shear rate Newtonian behaviour, the predictions of the flow are widely different from the predictions made using the power-law model.

Finally, the results of this study show that for some shear-thinning materials (hydroxyethylcellulose) the shear rate can become so large that the viscosity can vary by orders of magnitude within the transition region. For example, in figure 7(a) the dimensional shear rate reaches a value of a couple of thousand per second. The results support the argument put forth in § 1 that there is the possibility that a second high-shear rate transition occurs and that the Carreau model could be used to account for this behaviour. However, such a study has not been carried out for the reasons listed.

5. Conclusions

In this work, the thinning of lamella in two-dimensional surfactant-free foams having a non-Newtonian liquid phase is derived using matched asymptotic analyses in capillary number. Two generalized Newtonian liquid models, (i) the power-law model and (ii) the Ellis model are used in the analysis. According to the power-law model, in shear-thinning fluids, the viscosity is singular at the transition–lamellar region boundary and at the transition–Plateau boundary. Nevertheless, the fluid velocities, the foam gas–liquid interface shape and the pressure are well behaved throughout. The Ellis model does not exhibit a singularity in the viscosity.

One important finding of the analysis is that the variation in shear rate within the transition region renders the matching condition at the transition–Plateau boundary non-local. This result is in contrast to the local matching condition derived for the case of a Newtonian fluid in which the viscosity is constant throughout. Thus, numerical methods are developed to solve the equation for the transition-region shape and all other quantities that are used in determining the thinning law for the liquid lamellae.

Thinning rates are calculated for different fluids. In all cases considered, the thinning rates exhibit an initial transient acceleration over approximately two orders of magnitude of lamellar thinning from the initial film thickness, before settling into t^{-2} behaviour at longer times.

There are two types of foam, 'semi-arid' and 'arid', representing distinct asymptotic limits (Brush & Davis 2005). In semi-arid foam with power-law viscosity, a time constant can be chosen so that the thinning rates are independent of the two power-law parameters k and n. The power-law semi-arid foam obeys the same dynamical equation as a Newtonian foam. The semi-arid Ellis-model foam also exhibits the same behaviour. Thus, the change in time scale is the dominant leading-order effect in semi-arid foam thinning, pointing to the existence of an effective viscosity that may be used to monitor film thinning rates. This result is consistent with the results of Safouane *et al.* (2006) who showed in forced drainage experiments performed on a number of non-Newtonian foaming solutions that an effective viscosity can be identified in which the velocity of draining is the same as in a Newtonian fluid.

For the arid foam, in which the volume fraction of liquid is asymptotically smaller than the semi-arid foam and the radius of curvature of the Plateau border adjusts to the flow of incoming fluid from the thinning film, the thinning rate depends explicitly on the parameters defining the viscosity.

The Ellis model of viscosity avoids a singularity in the viscosity by including a low-shear-rate Newtonian Plateau. Calculations of the thinning rates are more complicated in the case of the Ellis model than in the power-law model, since they require the simultaneous solutions of multiple equations governing the transition-region shape and the viscosity. The Ellis model is shown to provide two scaling regimes for the viscosity in the transition region. The zero-shear-rate viscosity is appropriate for foams in which the shear rate is low enough throughout the transition region that the viscosity remains near the critical value marking the switch from Newtonian to power-law behaviour. For foams in which the shear rates are much larger, a different scaling for the viscosity is more appropriate, since the Ellis model exhibits power-law behaviour virtually throughout the transition region.

Calculations have been carried out for hydroxytheylcellulose, polysytrene, blood, a fictitious shear-thickening foam liquid and a Newtonian foam. In all cases, dimensional thinning rates are heavily dependent on the magnitude of the viscosity throughout the transition region. The larger the viscosity, the slower the thinning rate. However, conclusions regarding the stability of foam lamellae cannot be made based on thinning rate alone.

This work shows how a leading-order matched asymptotic analysis can be used to calculate interface shapes and viscous profiles in a self-consistent manner even for more complex rheologies than simple Newtonian foam. The transition-region dynamics dictate the rate of thinning, hence this has required the need to account for and to model the shear rate and variation in the viscosity in this region. The results are consistent with reported experimental results and provide insight into the reasons for the observed behaviour.

The authors gratefully acknowledge S. H. Davis for discussions and critical reading of the manuscript. SMR acknowledges support from MEANS II AFOSR Grant No. FA 9550-05-1-0089 and NSF Grant No. DMI-0507053.

Appendix A

Equation (3.48) is factored,

$$\frac{1}{\overline{\delta}}\left[H_{\hat{X}\hat{X}}H-\frac{1}{2}H_{\hat{X}}^{2}\right]_{\hat{X}}+4\left(\tilde{\eta}HU_{\hat{X}}^{(0)}\right)_{\hat{X}}=0, \tag{A 1}$$

and integrated to give

$$\frac{1}{\overline{\delta}}\left[H_{\hat{X}\hat{X}}H-\frac{1}{2}H_{\hat{X}}^{2}\right]+4\tilde{\eta}HU_{\hat{X}}^{(0)}=C_{1}. \tag{A 2}$$

$C_1=0$ since in the limit $\hat{X}\to-\infty$ all shape derivatives vanish. Substituting $U^{(0)}=\overline{Q}/H$ and multiplying by $H^{-3/2}$ gives

$$\frac{1}{\overline{\delta}}\left[H_{\hat{X}\hat{X}}H^{-1/2}-\frac{1}{2}\left(H_{\hat{X}}^{2}\right)H^{-3/2}\right]-4\tilde{\eta}\overline{Q}\frac{H_{\hat{X}}}{H^{5/2}}=0. \tag{A 3}$$

Equation (A 3) may be rewritten as

$$\frac{1}{\overline{\delta}}\left(H_{\hat{X}}H^{-1/2}\right)_{\hat{X}}+\frac{8}{3}\tilde{\eta}\overline{Q}\left(H^{-3/2}\right)_{\hat{X}}=0. \tag{A 4}$$

Let $\widehat{Q}=\overline{Q\delta}$. Integrating (A 4) gives

$$H_{\hat{X}}H^{-1/2}+\frac{8}{3}\widehat{Q}\int^{\hat{X}}\tilde{\eta}\left(H^{-3/2}\right)_{\hat{X}'}\mathrm{d}\hat{X}'=C_{2}, \tag{A 5}$$

where $\hat{X}'$ denotes a dummy integration variable. C_2 is defined by taking the limit $\hat{X}\to-\infty$ so that

$$C_{2}=\frac{8}{3}\widehat{Q}\lim_{\hat{X}\to-\infty}\left[\int^{\hat{X}}\tilde{\eta}\left(H^{-3/2}\right)_{\hat{X}'}\mathrm{d}\hat{X}'\right]\equiv\frac{8}{3}\widehat{Q}\tilde{\eta}_{-\infty}H_{L}^{-3/2}, \tag{A 6}$$

where H_L is the lamellar thickness, which is the value attained by H as $\hat{X}\to-\infty$. Integrating by parts gives:

$$H_{\hat{X}}H^{-1/2}+\frac{8}{3}\widehat{Q}\left[\tilde{\eta}H^{-3/2}-\int^{\hat{X}}\tilde{\eta}_{\hat{X}'}H^{-3/2}\mathrm{d}\hat{X}'\right]=C_{2}, \tag{A 7}$$

where all terms outside the integral are evaluated at $\hat{X}$, and $\tilde{\eta}_{\hat{X}'}$ is the derivative of $\tilde{\eta}\{\hat{X}'\}$ with respect to $\hat{X}'$. Thus,

$$H_{\hat{X}}H^{-1/2}+\frac{8}{3}\widehat{Q}\left[\tilde{\eta}H^{-3/2}-\tilde{\eta}_{-\infty}H_{L}^{-3/2}-\int^{\hat{X}}\tilde{\eta}_{\hat{X}'}H^{-3/2}\mathrm{d}\hat{X}'\right]=0. \tag{A 8}$$

Solving for $H_{\hat{X}}$,

$$H_{\hat{X}} = -\frac{8\widehat{Q}}{3H_L}\left[\tilde{\eta}\frac{H_L}{H} - \tilde{\eta}_{-\infty}\frac{H^{1/2}}{H_L^{1/2}}\right] + \frac{8\widehat{Q}}{3}H^{1/2}\left(\int^{\hat{X}}\tilde{\eta}_{\hat{X}'}H^{-3/2}\mathrm{d}\hat{X}'\right). \tag{A 9}$$

Differentiating $H_{\hat{X}}$,

$$H_{\hat{X}\hat{X}} = -\frac{8\widehat{Q}}{3H_L}\left[\tilde{\eta}_{\hat{X}}\frac{H_L}{H} - \tilde{\eta}\frac{H_L H_{\hat{X}}}{H^2} - \tilde{\eta}_{-\infty}\frac{H_{\hat{X}}}{2H^{1/2}H_L^{1/2}}\right] + \frac{8\widehat{Q}}{3}\left(\frac{H_{\hat{X}}}{2H^{1/2}}\right)\left(\int^{\hat{X}}\tilde{\eta}_{\hat{X}'}H^{-3/2}\mathrm{d}\hat{X}'\right) + \frac{8\widehat{Q}}{3}\left(\frac{\tilde{\eta}_{\hat{X}}}{H}\right). \tag{A 10}$$

The first and last terms on the right-hand side cancel. The remaining terms can be rearranged to give

$$H_{\hat{X}\hat{X}} = \frac{8\widehat{Q}}{3H_L}\left[\tilde{\eta}\frac{H_L H_{\hat{X}}}{H^2} + \tilde{\eta}_{-\infty}\frac{H_{\hat{X}}}{2H^{1/2}H_L^{1/2}}\right] + \frac{8\widehat{Q}}{3}\left(\frac{H_{\hat{X}}}{2H^{1/2}}\right)\left(\int^{\hat{X}}\tilde{\eta}_{\hat{X}'}H^{-3/2}\mathrm{d}\hat{X}'\right). \tag{A 11}$$

Factoring out $H_{\hat{X}}$,

$$H_{\hat{X}\hat{X}} = \frac{8\widehat{Q}}{3}\left[\frac{\tilde{\eta}}{H^2} + \frac{\tilde{\eta}_{-\infty}}{2H^{1/2}H_L^{3/2}} + \frac{1}{2H^{1/2}}\left(\int^{\hat{X}}\tilde{\eta}_{\hat{X}'}H^{-3/2}\mathrm{d}\hat{X}'\right)\right]H_{\hat{X}}. \tag{A 12}$$

Substituting in the expression for $H_{\hat{X}}$,

$$H_{\hat{X}\hat{X}} = \frac{8\widehat{Q}}{3}\left[\frac{\tilde{\eta}}{H^2} + \frac{\tilde{\eta}_{-\infty}}{2H^{1/2}H_L^{3/2}} + \frac{1}{2H^{1/2}}\left(\int^{\hat{X}}\tilde{\eta}_{\hat{X}'}H^{-3/2}\mathrm{d}\hat{X}'\right)\right] \times \frac{8\widehat{Q}}{3}\left[-\frac{\tilde{\eta}}{H} + \tilde{\eta}_{-\infty}\frac{H^{1/2}}{H_L^{3/2}} + H^{1/2}\left(\int^{\hat{X}}\tilde{\eta}_{\hat{X}'}H^{-3/2}\mathrm{d}\hat{X}'\right)\right]. \tag{A 13}$$

Multiplying,

$$\begin{aligned} H_{\hat{X}\hat{X}} = \left(\frac{8\widehat{Q}}{3}\right)^2 \Bigg[& -\frac{\tilde{\eta}^2}{H^3} - \frac{\tilde{\eta}\tilde{\eta}_{-\infty}}{2H^{3/2}H_L^{3/2}} + \frac{\tilde{\eta}\tilde{\eta}_{-\infty}}{H^{3/2}H_L^{3/2}} + \frac{\tilde{\eta}_{-\infty}^2}{2H_L^3} \\ & + \frac{\tilde{\eta}}{H^{3/2}}\left(\int^{\hat{X}}\tilde{\eta}_{\hat{X}'}H^{-3/2}\mathrm{d}\hat{X}'\right) + \frac{\tilde{\eta}_{-\infty}}{2H_L^{3/2}}\left(\int^{\hat{X}}\tilde{\eta}_{\hat{X}'}H^{-3/2}\mathrm{d}\hat{X}'\right) \\ & - \frac{\tilde{\eta}}{2H^{3/2}}\left(\int^{\hat{X}}\tilde{\eta}_{\hat{X}'}H^{-3/2}\mathrm{d}\hat{X}'\right) + \frac{\tilde{\eta}_{-\infty}}{2H_L^{3/2}}\left(\int^{\hat{X}}\tilde{\eta}_{\hat{X}'}H^{-3/2}\mathrm{d}\hat{X}'\right) \\ & + \frac{1}{2}\left(\int^{\hat{X}}\tilde{\eta}_{\hat{X}'}H^{-3/2}\mathrm{d}\hat{X}'\right)^2\Bigg], \end{aligned} \tag{A 14}$$

which upon factoring out H_L^3 and grouping terms becomes

$$H_{\hat{X}\hat{X}} = \left(\frac{8\widehat{Q}}{3H_L^{3/2}}\right)^2 \left[\frac{\tilde{\eta}_{-\infty}^2}{2} + \frac{\tilde{\eta}\tilde{\eta}_{-\infty}}{2}\left[\frac{H_L}{H}\right]^{3/2} - \tilde{\eta}^2\left[\frac{H_L}{H}\right]^3 + \frac{\tilde{\eta}}{2}\left[\frac{H_L}{H}\right]^{3/2}\left(\int^{\hat{X}} \tilde{\eta}_{\hat{X}'}\left[\frac{H_L}{H}\right]^{3/2} \mathrm{d}\hat{X}'\right) + \tilde{\eta}_{-\infty}\left(\int^{\hat{X}} \tilde{\eta}_{\hat{X}'}\left[\frac{H_L}{H}\right]^{3/2} \mathrm{d}\hat{X}'\right) + \frac{1}{2}\left(\int^{\hat{X}} \tilde{\eta}_{\hat{X}'}\left[\frac{H_L}{H}\right]^{3/2} \mathrm{d}\hat{X}'\right)^2\right]. \tag{A 15}$$

Finally, in the limit as $\hat{X} \to +\infty$, the ratio of $H_L/H \to 0$ which leaves

$$H_{\hat{X}\hat{X}} = \left(\frac{8\widehat{Q}}{3H_L^{3/2}}\right)^2 \left[\frac{\tilde{\eta}_{-\infty}^2}{2} + \lim_{\hat{X}\to\infty}\left[\tilde{\eta}_{-\infty}\left(\int^{\hat{X}} \tilde{\eta}_{\hat{X}'}\left[\frac{H_L}{H}\right]^{3/2} \mathrm{d}\hat{X}'\right) + \frac{1}{2}\left(\int^{\hat{X}} \tilde{\eta}_{\hat{X}'}\left[\frac{H_L}{H}\right]^{3/2} \mathrm{d}\hat{X}'\right)^2\right]\right]. \tag{A 16}$$

The first term on the right-hand side reduces to the appropriate limit if the liquid is Newtonian. The last two integrals are constant in this limit, but are not evaluable without knowledge of the *entire* transition-region shape. Defining the constant

$$D = \lim_{\hat{X}\to\infty}\left[\tilde{\eta}_{-\infty}\left(\int^{\hat{X}} \tilde{\eta}_{\hat{X}'}\left[\frac{H_L}{H}\right]^{3/2} \mathrm{d}\hat{X}'\right) + \frac{1}{2}\left(\int^{\hat{X}} \tilde{\eta}_{\hat{X}'}\left[\frac{H_L}{H}\right]^{3/2} \mathrm{d}\hat{X}'\right)^2\right], \tag{A 17}$$

the approximate shape of the transition region at the transition region/Plateau border boundary can be determined by integrating (A 16) in $\hat{X}$. The result is

$$H = \left(\frac{8\widehat{Q}}{3H_L^{3/2}}\right)^2 \left[\frac{\tilde{\eta}_{-\infty}^2}{2} + D\right]\frac{\hat{X}^2}{2} + A_1\hat{X} + A_2 \tag{A 18}$$

revealing that, through D, the variable viscosity helps determine the magnitude of the curvature at the transition Plateau border boundary at leading order.

Appendix B

The transition-region interface shape H and the Plateau border interface shape $\tilde{h}$ derived in the text are each leading-order terms of asymptotic expansions. Matching is accomplished by introducing the intermediate variable, $X_\nu = (X - L)/\nu$, such that $\delta \ll \nu \ll 1$, and writing the Plateau border and the transition region coordinates in terms of the intermediate variable (Kevorkian & Cole 1985):

$$x = L + \nu X_\nu, \text{ and } \hat{X} = \frac{\nu}{\delta}X_\nu. \tag{B 1}$$

At each order 'n' $= 0, 1, \ldots,$ (corresponding to the order of the asymptotic expansions of the interface shapes), the following conditions hold:

$$\lim_{\delta\to 0,\, X_\nu \text{ fixed}}\left[\frac{\tilde{h}^{(n)}(L + \nu X_\nu, \cdot)/\epsilon - H^{(n)}((\nu/\delta)X_\nu, \cdot)}{\delta^n}\right] = 0. \tag{B 2}$$

Here, we only consider the leading-order terms in the asymptotic solutions for the shapes i.e. (3.9) and (A 18). Substituting these solutions into (B 2) for $n=0$ gives

$$\lim_{\delta\to 0,\ X_\nu \text{ fixed}} \left[\frac{h_{ol}}{\epsilon} + \frac{\tilde{a}}{\epsilon}\left(1-\frac{1}{\sqrt{2}}\right) - \frac{1}{\sqrt{2}\Delta P\epsilon} + \frac{1}{\epsilon\Delta P}\left\{1-\left[\frac{1}{\sqrt{2}} - \Delta P\left(\nu X_\nu - \frac{\tilde{a}}{\sqrt{2}}\right)\right]^2\right\}^{1/2} - \left(\frac{8\widehat{Q}}{3H_L^{3/2}}\right)^2 \left[\frac{\tilde{\eta}_{-\infty}^2}{2} + D\right] \frac{\nu^2 X_\nu^2}{2\delta^2} - A_1 \frac{\nu X_\nu}{\delta} - A_2 \right] = 0. \tag{B 3}$$

Expanding the square root at small ν gives

$$\lim_{\delta\to 0,\ X_\nu \text{ fixed}} \left[\frac{h_{ol}}{\epsilon} + \frac{\tilde{a}}{\epsilon}\left(1-\frac{1}{\sqrt{2}}\right) - \frac{1}{\sqrt{2}\Delta P\epsilon} - \frac{\left[1-4\tilde{a}\Delta P + 2\tilde{a}^2\Delta P^2 + 4\tilde{a}^3\Delta P^3 + \tilde{a}^4\Delta P^4\right]}{\left[\sqrt{2}\epsilon\Delta P\left(1-2\tilde{a}\Delta P - \tilde{a}^2\Delta P^2\right)^{3/2}\right]} - \frac{(\sqrt{2}\nu X_\nu \Delta P\left[(1-\tilde{a}\Delta P - 3\tilde{a}^2\Delta P^2 - \tilde{a}^3\Delta P^3)\right] - (2(\nu X_\nu \Delta P)^2))}{\left[\sqrt{2}\epsilon\Delta P(1-2\tilde{a}\Delta P - \tilde{a}^2\Delta P^2)^{3/2}\right]} - \left(\frac{8\widehat{Q}}{3H_L^{3/2}}\right)^2 \left[\frac{\tilde{\eta}_{-\infty}^2}{2} + D\right] \frac{\nu^2 X_\nu^2}{2\delta^2} - A_1 \frac{\nu X_\nu}{\delta} - A_2 + \cdots \right] = 0. \tag{B 4}$$

The choice $\Delta P \equiv -1/\tilde{a}$ is made, so that the leading-order Plateau border shape obeys the Young–Laplace equation. The matching condition becomes

$$\frac{h_{ol}}{\epsilon} - A_2 - A_1\frac{\nu X_\nu}{\delta} + \frac{(\nu X_\nu)^2}{2\epsilon\tilde{a}} - \left(\frac{8\widehat{Q}}{3H_L^{3/2}}\right)^2 \left[\frac{\tilde{\eta}_{-\infty}^2}{2} + D\right] \frac{\nu^2 X_\nu^2}{2\delta^2} = 0. \tag{B 5}$$

From (B 5), the following conclusions are reached. First, $A_2 = h_{ol}/\epsilon$, so that the thicknesses of the transition and Plateau border regions match for $h_{ol} \sim O(\epsilon)$. Second, A_1 vanishes at leading order, thereby fixing the relative lateral positions of the transition and the Plateau borders. Thus,

$$\frac{1}{\epsilon\tilde{a}} = \left(\frac{8\widehat{Q}}{3H_L^{3/2}}\right)^2 \left[\frac{\tilde{\eta}_{-\infty}^2}{2} + D\right] \frac{1}{\delta^2}, \tag{B 6}$$

which is a leading-order matching condition for the curvatures of the transition and the Plateau border regions.

REFERENCES

Banhart, J. 2001 Manufacture, characterization, and application of cellular metals and metal foams. *Prog. Mater. Sci.* **46**, 559.

Bird, R. B., Armstrong, R. C. & Hassager, O. 1977 *Dynamics of Polymeric Fluids, Vol. I – Fluid Mechanics*. John Wiley and Sons.

Breward, C. J. W. 1999 The mathematics of foam. DPhil thesis. Oxford University.

Breward, C. J. W. & Howell, P. D. 2002 The drainage of a foam lamella. *J. Fluid Mech.* **458**, 379–406.

Brush, L. N. & Davis, S. H. 2005 A new law of lamellar thinning in foam. *J. Fluid Mech.* **534**, 227–236.

Erneux, E. & Davis, S. H. 1993 Nonlinear rupture of free films. *Phys. Fluids* A **5**, 1117–1122.

Hamdorf, M. & Johannsmann, D. 2000 Surface-rheological measurements on glass forming polymers based on the surface tension driven decay of imprinted corrugation gratings. *J. Chem. Phys.* **112**, 4262–4270.

Howell, P. D. 1999 The draining of a two dimensional bubble. *J. Engng Maths* **35**, 251–272.

Hrncir, E. & Rosin, J. 1997 Surface tension of blood. *Physiol. Res.* **46**, 319–321.

Kevorkian, J. & Cole, J. D. 1985 *Perturbation Methods in Applied Mathematics.* Springer.

Myers, T. G. 2005 Application of non-Newtonian models to thin film flow. *Phys. Rev.* E **72**, 066302.

Rosenblatt, S. & Davis, S. H. 1984 How do liquid drops spread on solids? In *Frontiers in Fluid Mechanics* (ed. S. H. Davis & J. L. Lumley), vol. 171. Springer.

Safouane, M., Saint-Jalmes, M., Bergeron, V. & Langevin, D. 2006 Viscosity effects in foam drainage: Newtonian and non-Newtonian foaming fluids. *Eur. Phy. J.* E **19**, 195–202.

Scheffler, M., Gambaryan-Roisman, T., Zeschky, J., Scheffler F. & Greil, P. 2002 Self-foamed cellular ceramics from solicone resins with a zeolite surface. *Ceram. Engng Sci. Proc.* **23**, 203–210.

Wang, Z. & Narsimhan, G. 2006 Model for Plateau border drainage of power-law fluid with mobile interface and its application to foam drainage. *J. Colloid Interface Sci.* **300**, 327–337.

Yang, C. C. & Nakae, H. 2003 The effects of viscosity and cooling conditions on the foamability of aluminum alloy. *J. Mat. Proc. Tech.* **141**, 202–206.